Review

Israel Journal of Chemistry

DOI: 10.1002/ijch.201900116

Review of Computational Studies of NCM Cathode Materials for Li-ion Batteries

Arup Chakraborty[+],[a] Sooraj Kunnikuruvan[+],[a] Mudit Dixit,[a, b] and Dan T. Major*[a]

Abstract: Lithium-ion based rechargeable batteries are considered among the most promising battery technologies because of the high energy- and power-densities of these electrochemical devices. Computational studies on lithium ion batteries (LIBs) facilitate rationalization and prediction of many important experimentally observed properties, including atomic structure, thermal stability, electronic structure, ion diffusion pathways, equilibrium cell voltage, electrochemical activity, and surface behavior of electrode materials. In recent years, Ni, Co and Mn-based (NCM) layered transition metal oxide positive electrode materials ($LiNi_{1-x-y}Co_xMn_yO_2$) have shown tremendous promise for high-energy density LIBs, and these NCM-based batteries are effectively commercialized. Here, we present an overview of recent theoretical work performed using first principles density functional theory on these layered cathode materials. This short review focuses on recent computational efforts of popular NCMs with increasing Ni content, ranging from NCM333 to NCM811.

Keywords: Li-ion battery · cathode materials · computational study · layered oxides · NCM

1. Introduction

An ever-increasing global demand for energy, continuous depletion of conventional fossil fuels, and increasing production of CO_2 necessitate the development of efficient green and renewable energy sources.[1] Although the renewable energy sources, such as solar, wind, and tide can contribute to our current global energy needs to a significant extent, the energy production from these resources depends on the climate and geographical changes.[1a,b,d–f] Thus, the practical application of these naturally available resources is limited and not equally applicable everywhere.

Among various promising and environmental-benign energy resources developed so far, rechargeable battery technology is the most sought-after due to its portability, good energy and power density, cost-effectiveness, and safety properties compared to other energy sources.[1c,f,2] Lithium ion batteries (LIB) have been successfully commercialized for portable electronic devices since 1991.[3] The superior electrochemical performance of LIBs in comparison to other rechargeable batteries are largely due to the special properties of Li: small size and a low reduction potential (−3.04 V with respect to standard hydrogen electrode).[4] The importance of LIB is underscored by this year's (2019) Nobel prize in chemistry, which was awarded to Prof. J. B. Goodenough, Prof. M. Stanley Whittingham, and Prof. Akira Yoshino for their contribution to development of rechargeable LIBs.

Li intercalated transition metal (TM) oxide-based electrodes and graphitic electrodes with alkyl carbonates are widely used as cathode, anode and electrolyte materials, respectively, in LIBs.[3a,b,e,f,5] Though, Li metal anode can provide high specific capacity, the safety issues associated with this anode due to dendrite formation prevent the use of this anode.[5m,6] Commonly used graphite anodes have been studied extensively, and have a capacity that is close to the theoretical one.[7] Therefore, most studies on LIBs in recent years have focused on the development of cathode materials.[3e,f,h–j,5a,d–h,j,k,8]

Based on the crystal structure, cathode materials for LIBs can be classified into layered, spinel, olivine, and polyanionic fluoro-phosphate, tavorite materials.[3e,9] Among these, layered cathode materials are currently most promising due to their high energy density, as exemplified by the commercialization of several LIBs with layered cathodes.[3d,e,8c] The general formula for layered cathode materials belonging to the *R-3m* space group is $LiMO_2$, where M is a transition metal, with an α-$NaFeO_2$-like structure.[9a,10] $LiMO_2$ consists of alternating layers of Li and M within a tetrahedral or octahedral arrangement of oxygen atoms.

In 1980, Goodenough introduced one of the basic $LiMO_2$ materials, $LiCoO_2$ (LCO),[11] which was later commercialized by Sony.[3d] LCO has a theoretical capacity of 274 mAh g^{-1} but the practical capacity of this material was found to be about half of this (135 mAh g^{-1} in a voltage window of 3.0–4.2 V).[3f] Moreover, LCO was found to undergo significant capacity fading on cycling.[3j,12] Another crucial issue associated with this material is the low abundance and high cost of

[a] *A. Chakraborty,[+] S. Kunnikuruvan,[+] M. Dixit, D. T. Major*
Department of Chemistry and Institute for Nanotechnology & Advanced Materials, Bar-Ilan University, Ramat-Gan 52900, Israel
Tel. + 972 3 531 73 92; Fax. + 972 3 738 40 53
E-mail: majort@biu.ac.il
[b] *M. Dixit*
Division of Research & Development, Lovely Professional University, Phagwara 144411, Punjab, India
[+] *These authors contributed equally.*

Co. These drawbacks of LCO led to the development of comparatively cheaper Ni-based $LiMO_2$ material, i.e. $LiNiO_2$ (LNO).[13] The theoretical capacity of LNO is comparable (275 $mAh\,g^{-1}$) to LCO but its practical capacity (150 $mAh\,g^{-1}$ in a voltage window of 2.5–4.2 V) was found to be higher relative to LCO.[3e,13b,14] However, LNO also suffers from poor cycling performance, ascribed to structural changes occurring during charge-discharge. Moreover, LNO materials are known to have anti-site defects known as cation disorder, where some of the Ni atoms from the TM layer migrate to the Li-layer due to the comparable size of Li^+ and Ni^{2+} ions.[8b,15] The presence of Ni in the Li-layers adversely affects Li-diffusion.[8a,16] $LiMnO_2$ (LMO) is another basic well studied $LiMO_2$ material, with the advantage that Mn is relatively cheaper than both Ni and Co. This material has a theoretical capacity of 285 $mAh\,g^{-1}$ and a practical capacity of 200 $mAh\,g^{-1}$ (in a voltage window of 2.5–4.3 V).[3e] However, LMO undergoes a layered structure to spinel transition during cycling, which in turn results in very rapid capacity fading.[5d,17] Moreover, the formation of spinel structure divides the operational potential into two domains (either lower or higher potential only) due to the Jahn-Teller distortion-assisted structural changes for continuous potential window.[18] This reduces the practical capacity of LMO to half in each voltage window ($<$ 120 $mAh\,g^{-1}$). In addition to this, Mn ions in LMO were found to migrate to the anode and has an adverse effect on the electrode passivation layer.[19] Among these three basic layered materials, LCO and LNO have a *R-3m* rhombohedral structure, whereas LMO has a *Pmmn* orthorhombic structure.[9a,10]

In order to improve the electrochemical performance of basic $LiMO_2$ materials, mixing of different transition metal oxides to form binary and ternary TM oxides was found to be a good strategy.[8b,20] Among various mixed transition metal oxide materials developed as cathodes for LIBs, the ones with Ni, Co and Mn (NCM) and Ni, Co and Al (NCA) were found to be very promising.[3f,5k,8b] These materials have a practical capacity of 200–210 $mAh\,g^{-1}$ (in a voltage window of 3–4.3 V).[3f,5k,8b] In these mixed transition metal oxides, Ni, Co and Mn/Al are chosen due to their ability to improve capacity, charge-discharge kinetics and structural stability,

Arup Chakraborty obtained his M.Sc. in Physics from Visva-Bharati University, Shantiniketan, India. He received his Ph.D. degree in Theoretical Physics from Indian Association for the Cultivation of Science (IACS), Kolkata, India under The University of Calcutta. He is currently working as a post-doctoral fellow at Bar-Ilan University, Israel, under the guidance of Prof. Dan T. Major. His research primarily focuses on computational studies of cathode materials for Li-ion batteries and novel nanostructures.

Sooraj Kunnikuruvan obtained his M.Sc. degree in Chemistry from Mahatma Gandhi University, India. He received a Ph. D. degree in computational chemistry from Indian Institute of Technology Kanpur, India. Currently, he is a post-doctoral fellow at Bar-Ilan University, Israel, under the guidance of Prof. Dan T. Major. His research areas include computational studies on electrochemical properties of cathode materials for batteries and development of novel computational approaches with application to materials simulations.

Mudit Dixit completed his M.Sc. in Chemical Sciences at Pondicherry University in 2008. He received his Ph.D. from CSIR-National Chemical Laboratory, India, under the supervision of Prof. Sourav Pal. During his postdoctoral work at the Department of Chemistry (2013–2017) at Bar-Ilan University, Israel, he worked on understanding and designing advanced cathode materials for Li/Na batteries, and Bio-catalysis of enzymes under the supervision of Prof. Dan T. Major. In his next postdoctoral appointment (2017-2019) at the Chemical Petroleum Engineering Department at the University of Pittsburgh, USA, he worked on heterogeneous catalysis under the supervision of Prof. Giannis Mpourmpakis. He recently joined Lovely Professional University, India as an Assistant Professor. His main research interests are in the field of computational electrochemical energy storage and heterogeneous catalysis.

Prof. Dan T. Major completed his undergraduate studies in chemistry and computer sciences at Bar-Ilan University in 1997. He received his Ph.D. from Bar-Ilan University in 2003 under Prof. Bilha Fischer. During his Ph.D. he worked on molecular properties of nucleotide derivatives, theoretical modeling of G-protein coupled receptors, as well as molecular recognition. He did a post-doctorate at the University of Minnesota under Prof. Jiali Gao during the years 2003–2006. During his post-doctorate he was involved in development and application of theoretical methods for enzyme catalysis. Since 2007 he is a Faculty member in the Chemistry Department at Bar-Ilan University. His main research interests are in the field of computational chemistry, computational biochemistry, and computational nanotechnology.

respectively.[21]

NCM and NCA materials with varying Ni, Co and Mn/Al have been studied over the years.[3f,8b] These studies indicate that Ni-rich materials are ideal candidates for high-capacity batteries.[3f,5d,f,k,8b,21–22] However, charge-discharge kinetics and material stability of these materials remains a concern, as for LNO, and large numbers of studies have been devoted to understanding capacity fading in Ni-rich NCMs and NCAs.[23] The maximum efficiency of NCM cathode materials are found to be affected by Li–Ni exchange, phase transition, crack propagation, and oxygen evolution. The crucial factors for these phenomena are the Ni concentrations and depth of charge.[24] Doping and surface coating are two widely used strategies for improving the structural stability as well as electrochemical properties of these materials.[3f,5d,k,25] Various dopants such as Al, Ag, Mg, W, Ti, Nb, Ta, B, Mo, and Zr have been used in layered cathode materials to improve their properties.[25b,26]

Computational studies play an important role in the development of these electrode materials for battery applications.[9b,27] Various properties such as structure, electronic structure, voltage, ion diffusion, thermal and electrochemical stability, oxidation state of TM ions, effect of doping, and surface properties can be calculated using various computational approaches.[9b,21b,25g,26f,l,27a–d,28] Density functional theory (DFT) based computations have been very successful in reproducing and predicting experimental observations and have been used for studying properties of cathode materials, especially of layered materials, since the late 1990s.[27d] The constant increase in computational facilities and new developments in the field of computational chemistry over the years have made *in silico*-assisted design of cathode materials an important research direction.

Excellent reviews focusing on the role of computational studies on the development of electrode materials can be found elsewhere.[9b,27a,d,e,29] In this review, we focus only on computational studies reported on NCM materials, with special focus on our own work. Here, we will discuss several important properties of different NCMs, such as ionic structure, electronic structure, voltage profiles, ion diffusion, doping and surface properties and computational approaches used to obtain these properties.

2. Properties of NCM

2.1 Structural Properties

The structure of layered metal oxide cathode materials has a prototype of α-$NaFeO_2$.[5a,10,20a,30] Li-based layered metal oxides have rhombohedral structure with space group *R-3m*, where Li and TMs are arranged in alternating layers in perpendicular direction to its plane.[5a,10,20a,30] In NCM layered materials, one of the greatest challenges for theoreticians and experimentalist alike is to determine the proper distribution of Ni, Co, and Mn TMs in the layers. In the following, we discuss computational approaches for finding the structures of different NCMs.

2.1.1 Methods

Different computational methods to determine the ionic structure of layered materials have appeared in the literature, such as cluster expansion (CE) or classical simulations like Monte-Carlo simulated annealing (MCSA).[9b,31] The CE method is based on the Ising model and lattice sites are described by different possible clusters, like monomers, dimers, trimers, etc. and the interaction between these clusters contribute to the total energy of the system.[31b,c] Molecular mechanics (MM) or classical force fields (FF) are cost-effective ways to model ionic distribution, in conjunction with classical simulation techniques.[9b,32] DFT can also be used to score different layered structures, but is often limited to a relatively small number of ionic configurations due to the high computational cost.

2.1.2 Structure of NCM

Pristine NCM with equal concentration of Ni, Co and Mn (NCM333, $LiNi_{0.33}Co_{0.33}Mn_{0.33}O_2$) in the fully lithiated limit conforms with the *R-3m* space group and there are several possible distribution of the TMs, as found from computational and NMR spectroscopy studies.[33] Different groups showed $[\sqrt{3}\times\sqrt{3}]$ R30° structures in the TM layer of NCM333 (see Figure 1(a)).[30c,33b] It was found that DFT within the GGA and hybrid HSE06 approximations give good agreement with experimental lattice parameters (a = b = 8.56 Å and c = 14.23 Å) of NCM333.[34] Dixit et al. used a funneled search approach to find the lowest energy ionic configurations and found patterns very similar to $[\sqrt{3}\times\sqrt{3}]$ for NCM523, NCM622, NCM811, as shown in Figure 1 (b), (c), and (d), respectively.[21b,26f,l,28d] We note that for Ni-rich materials it is challenging to find exact $[\sqrt{3}\times\sqrt{3}]$ patterns similar to NCM333, since the concentration of Co, Mn is relatively low compared to the concentration of Ni.

It is important to note that the change in lattice parameter *c* shows a characteristic dip with delithiation but standard methods like PBE and PBE + *U* can't reproduce this behavior, whereas PBE and PBE + *U* with dispersion corrections, as well as the newly developed SCAN functional can properly describe it.[26l,28d,35]

2.2 Electronic Structure

The physical and chemical properties of a material system are largely determined by its electronic structure. Density of states (DOS) has been known to reveal fine electrochemical details of materials.[28d,35]

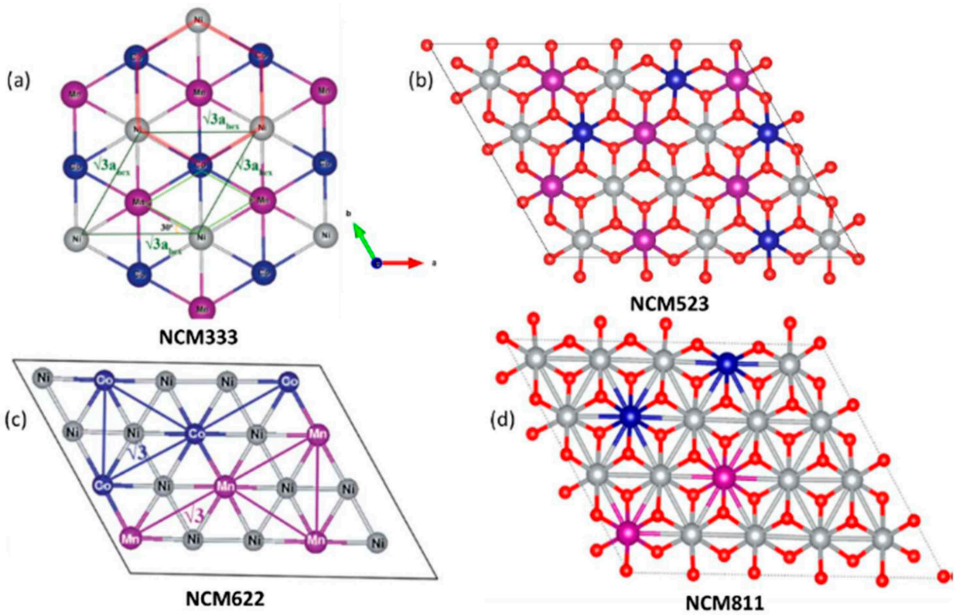

Figure 1. Pattern of distribution of Ni, Co, Mn in (a)NCM333, (b) NCM523, (c) NCM622, (d) NCM811. Color codes for spheres: Ni-Grey, Co-Blue, Mn–Magenta, O-Red (Reproduced from Ref. [21b, 26l, 28d] with permission from the Royal Society of Chemistry and American Chemical Society).

2.2.1 Methods

DFT is currently the best choice for calculation of the electronic structure of cathode materials. The limitation of DFT is confined to the exchange-correlation (xc) interaction between electrons. Different popular xc functionals, such as LDA and GGA are known to underestimate some of the key properties like band gap, magnetic moment, voltage, and change in lattice parameter *c* with delithiation However, addition of a Hubbard parameter to GGA (i. e. GGA + *U*) with dispersion corrections, as well as the newly developed SCAN meta-GGA functional perform better for these key properties.[35–36] We note that the choice of the Hubbard *U* parameter is crucial for the calculation of properties of NCM cathode materials.[35,37] The commonly applied effective *U* parameters for Ni, Co and Mn are 5.96, 5.00 and 5.10 eV, respectively. For dopants, such as for Mo, the applied effective *U* is 5 eV.[21b,26b,f,28d,38]

2.2.2 Electronic Structure of NCM

From calculation of the electronic structure, we can readily identify the spin state of the TMs in NCM.[21b,26b,l,28d] In pristine NCM, Ni ions are present in three different oxidation states, e. g. 2+, 3+, and 4+. Co ions are usually found in a low spin (LS) state and mostly in a 3+ oxidation state.[21b,26b,l, 28d] Mn ions usually exist as 4+ in a high-spin (HS) state.[21b,26b, l,28d] It is also important to note that antiferromagnetic spin configurations of TMs are usually more favorable than ferromagnetic configurations.[21b,26b,l,28d] The DOS of NCM333, NCM523, NCM424, NCM622, and NCM811 reveal that Ni ions are likely more chemically active than Co and Mn since Ni-*3d* states appear near the Fermi level and are hybridized with O-*2p*.[21b,26b,l,28d] Co-*3d* states are far from the Fermi level and show diamagnetic nature. It is also important to note that the amount of Ni^{3+} ions increases with increasing Ni content in NCMs while Ni^{2+} ion content decreases (Figure 2A). However, the presence of Jahn-Teller active Ni^{3+} ions could enhance the instability of the Ni-rich NCM.

Dixit et al. compared the electronic structure of different NCMs and found that the contribution of the Ni-t_{2g} states increases with Ni concentration in NCMs (Figure 2B). Based on the analysis of the DOS the authors revealed that the contribution of the Ni-e_g states decreases with increasing Ni concentration (Figure 2B, from NCM424 to NCM811). Additionally, the authors suggested that the metal-oxygen covalency increases with Ni content in Ni-rich NCMs, due to a shift of the Ni-bands toward the oxygen *2p* bonding bands (Figure 2B, orange box) and an increase in the Ni character in the oxygen *2p*-bonding peaks.

We note that the layered cathode materials, namely $LiCoO_2$, $LiNiO_2$, $LiMnO_2$, have band gaps of 2.7, 0.4 and 1.64 eV, respectively, and NCM333 or NCM424 have similarly small band gaps.[39] The band gaps of NCMs decrease with increasing Ni-content, as observed from DOS shown by Dixit et al. and Sun et al.[21b,40]

It was also demonstrated that in mixed transition metal oxides (such as NCMs), the electronic structure calculated using the PBE + *U* method (using the *U* values adopted for single TM oxides) shows large contribution of oxygen ions near the Fermi level (Figure 3), whereas TM *d*-states were

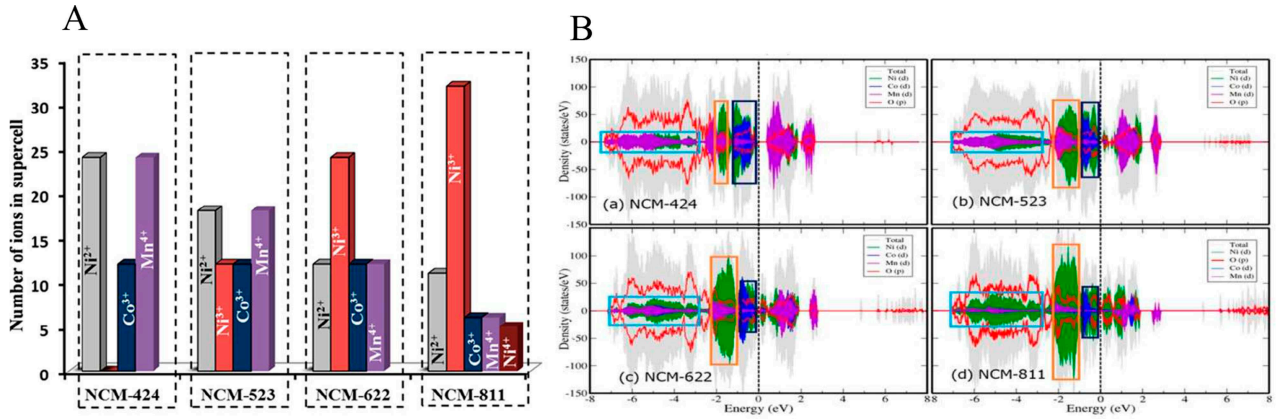

Figure 2. (A) The oxidation states of transition metal ions in various NCMs. (B) DOS for (a–d) NCM424, NCM523, NCM622 and NCM811, respectively. The center, right, and left boxes indicate the Ni-t_2g band, Ni-e_g band, and metal character in hybridized O-metal bonding states, respectively. (Reproduced from Refs. [21b] with permission from the American Chemical Society).

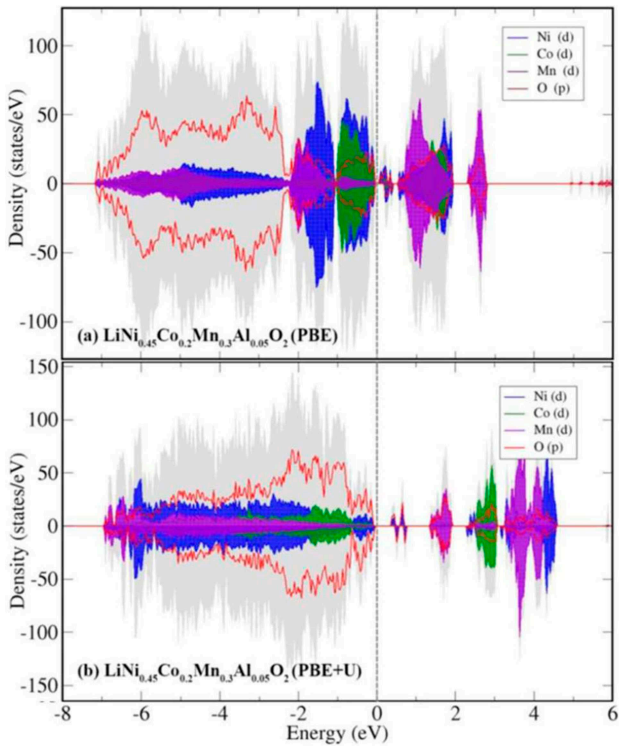

Figure 3. DOS for $LiNi_{0.45}Co_{0.2}Mn_{0.3}Al_{0.05}O_2$ using (a) PBE (b) PBE+*U*. Total DOS is shown in grey. (Reproduced from Ref.[26f] with permission from the Electrochemical Society).

found to be located considerably below the Fermi level, which is at odds with the electrochemical activity of these materials and classical TM redox behavior.[26f]

2.3 Intercalation Voltage

2.3.1 Methods

The intercalation voltage of a battery for a particular composition x is calculated from the difference in chemical potentials of anode and cathode using the following expression:[28a,b]

$$V(x) = \frac{\mu_{\text{anode}}(x) - \mu_{\text{cathode}}(x)}{z \cdot F}$$

Here, μ_{anode} and μ_{cathode} are the chemical potentials of the anode and cathode, respectively, z is the number of charge units transferred, and F is Faraday's constant. Since the energy density of the battery depends on the voltage, as well as the stability of the electrolyte, identification of cathode materials with high open circuit voltage (OCV) is crucial for the development of high energy density batteries.

Since, the chemical potentials are related to the change in free energy of the material, one can calculate the average equilibrium voltage, $\bar{V}$, using the expression,

$$\bar{V} = \frac{G_{\text{delithiated}} - G_{\text{lithiated}}}{\Delta x \cdot F}$$

Here, $G_{\text{lithiated}}$ and $G_{\text{delithiated}}$ are the free energies of the material in the fully lithiated and delithiated states, respectively, and Δx is the number of ions transferred. In practice, instead of free energies one can use the potential energy, E, as the entropy contribution to a solid electrode is generally small at room temperature. Thus, the above equation can be modified as,[28a,b]

$$\bar{V} = \frac{E_{\text{delithiated}} - E_{\text{lithiated}}}{\Delta x \cdot F}$$

Here, E can be obtained from first principle calculations. One can also generate the voltage profile using the same expression by calculating E for different delithiation levels, x, and this profile may be compared with the experimentally obtained one. We note that the computationally obtained voltage profile is generally plotted as a staircase-like curve, as each point of the voltage profile consists of values that are obtained by averaging two delithiated concentrations. In this case constant potentials are assigned to both of these concentrations, x. However, if the average potential at a given Li concentration is used instead then the resulting voltage profile is a smooth curve.[8,10–11] These calculations help to identify the ionic and electronic structural changes of the materials during delithiation, which is otherwise difficult to obtain from experiments due to the instability (or metastability) of many of the delithiated structures.

In one of the earliest computational studies on layered materials, Aydinol et al. used the LDA approach to compute the intercalation voltage of different $LiMO_2$ materials for various *3d* transition metals including Ni, Co, and Mn. The authors found that LDA can reproduce the trend of the experimental voltages for these materials, though the computed values were underestimated compared to the experimental voltages by ~1 V.[28a,b] We note that despite the underestimation of average voltages due to self-interaction error in the two-electron terms, both LDA and GGA methods have successfully predicted voltage trends of layered oxide materials.[41] The underestimation of the voltage by LDA and GGA can be corrected by using the GGA + U approach with an appropriate Hubbard U parameter.[9b,c,27d] However, employing a Hubbard U parameter to accurately calculate voltage profiles is problematic as an appropriate U value is determined by the extent of electron correlation, and for layered lithiated metal oxides (such as NCMs) the electron correlation changes with the level of lithiation (due to change in oxidation state of TMs with delithiation).[21b,26l,28d] Moreover, different Hubbard U values would preclude the calculation of any meaningful property as energy differences of two structures with different U values are not physically meaningful. Hybrid functionals such as HSE06, which can account for part of the self-interaction error, were also employed by various groups to study voltage profiles (Figure 4(A)).[27d,34,42] However, hybrid functionals are computationally expensive relative to LDA and GGA.[34,37,41e] Chakraborty et al. compared the performance of PBE, PBE + U and the recently developed SCAN functional, and found that the average voltages computed with SCAN are in better agreement with experiments for $LiMO_2$ (M=Ni, Co, Mn).[35] The improved performance of SCAN over GGA and GGA + U methods can be ascribed to its ability to account for localized states, as well as dispersion interactions.[35]

2.3.2 Study of Intercalation Voltages of NCM

Koyama et al. and Hwang et al. employed LDA and GGA approaches to calculate the average Li intercalation potential for NCM333 in good agreement with experiments (NCM has a rechargeable capacity of 163 mAh g^{-1} in the voltage window 3.0–4.3 V with 0.1 C rate).[30c] Studies by Koyama et al. and Hwang et al. also showed that the main redox processes in the Li concentration ranges $1 \geq x \geq 2/3$, $2/3 \geq x \geq 1/3$ and $1/3 \geq x \geq 0$ are oxidation of Ni^{2+} to Ni^{3+}, Ni^{3+} to Ni^{4+} and Co^{3+} to Co^{4+}, respectively.[30b] Using GGA and GGA + U methods, Markus et al.[41a] investigated the voltage profile of NCM333. The authors found that the GGA method underestimated the Li intercalation voltage by ~1 V. The authors attempted to calibrate the U-parameters against the experimental voltage profile of NCM333 but noted that the U values that

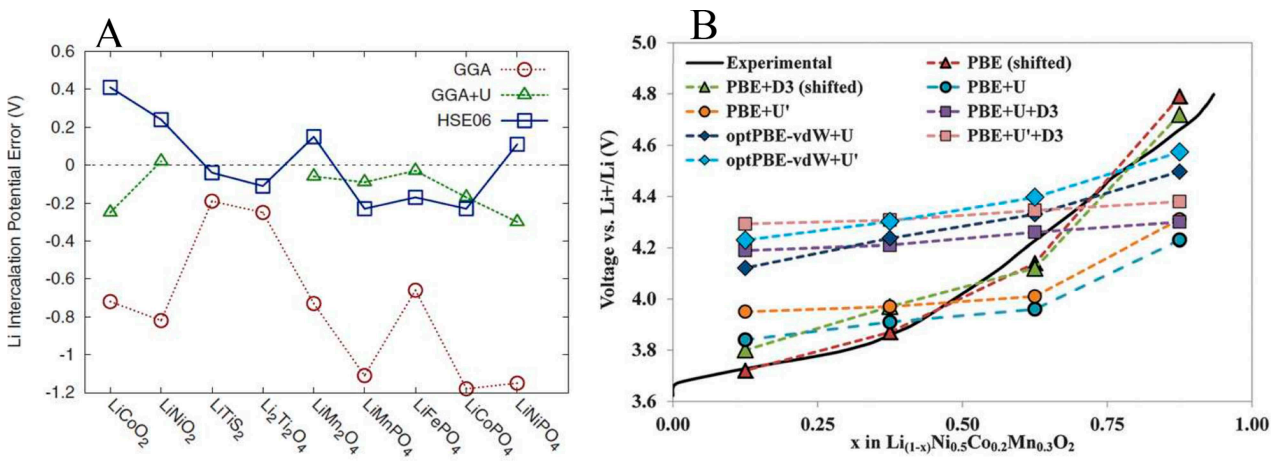

Figure 4. (A) Error in average Li-intercalation potentials (with respect to experimental values) for GGA, GGA + *U*, and HSE06 (Reproduced from Ref. [27d] with permission from the Nature Partner Journal). (B) Calculated and experimental intercalation potentials profile for $Li_xNi_{0.5}Co_{0.2}Mn_{0.3}O_2$ at different delithiation levels. GGA values are shifted by 0.9 eV and GGA + D3 are shifted by 0.6 eV. The black line represents the experimental data from Ref. [28d]. The experimental data are plotted by considering a specific capacity of 250 mAh g^{-1} in the fully delithiated limit. (Reproduced from Ref. [28d] with permission from the Royal Society of Chemistry)

give reasonably correct voltage profiles show incorrect redox behavior (e. g. Co was found to oxidize before Ni).

Dixit et al. compared the voltage profile of NCM523 obtained using PBE, PBE + U and PBE + U + D3 functional with experiments and found that PBE and PBE + D3 reproduce the experimental trends quite well, whereas PBE + U and PBE + U + D3 failed to reproduce the experimental voltage trends (Figure 4(B)).[28d] Though PBE + U failed to reproduce the experimental trends of the voltage profile, it was found that the absolute voltages calculated using PBE + U are in better agreement with experiments than PBE and PBE + D3. This study showed for NCM523 in the lower voltage limit ($x < 1/4$), oxidation of Ni^{2+} to Ni^{3+} is the main redox process, whereas at higher voltages, the redox process is dominated by Ni^{3+} to Ni^{4+} and Co^{3+} to Co^{4+} transitions.[28d]

Failure of PBE + U to reproduce the experimental voltage profile trends was also observed by Schipper et al. in their computational and experimental studies on NCM622 (initial discharge capacity of 187 mAh g^{-1} in the voltage window of 3.0 to 4.3 V).[26l] Their study showed that PBE and optPBE-vdW, which is a dispersion corrected version of PBE, reproduce the experimental trends whereas PBE + U fails to reproduce the experimental trends. The authors suggested that although PBE + U was unsuccessful in predicting the correct voltage profile trend, this is not due to the lack of accuracy of the PBE + U method itself. Rather this is due to the use of same U parameter irrespective of the change in Li concentration which results in changes in electron correlation.[26l]

Further, Susai et al. recently showed discharge capacity of 185–195 mAh g^{-1} for undoped and 1–3 mol% Mo-doped NCM811 in the voltage window of 2.8 to 4.3 V.[38] They also showed that Mo-doped NCM811 has reduced fading upon cycling from a combined experimental and computational approach.

2.4 Ion Diffusion

Understanding ion diffusion kinetics and diffusion mechanisms are crucial for the development of batteries with high-power density.[43] Here, ion diffusion within solid electrodes are particularly important due to the slow ion diffusion in electrodes compared to electrolytes. The nature of diffusion, i. e. how fast or slow the diffusion is, can be understood by looking at the ion diffusion coefficient, D, and it can be computed from both experiments and computational methods. However, experiments can only provide the total diffusion rate, while using theory one can calculate diffusion coefficients at electrodes, electrolyte and electrode-electrolyte interface and one can also pinpoint specific diffusion mechanisms.

2.4.1 Methods

Molecular dynamics (MD) simulations, kinetic Monte-Carlo (kMC) and nudged elastic bands (NEB) are common approaches used for the calculation of diffusion constants.[27d] From MD or kMC trajectories, the diffusion coefficient can be computed using mean square displacements (MSD) using the following expression:

$$D \approx \frac{\mathrm{MSD}}{2 \cdot d \cdot t}$$

Where,

$$\mathrm{MSD} = \sum_{I=1}^{N} \frac{1}{N} \langle |\mathbf{R}_I(t) - \mathbf{R}_I(t_0)|^2 \rangle$$

$\mathbf{R}_I(t)$ and $\mathbf{R}_I(t_0)$ are the positions of particle I at times t and t_0, respectively, and d is the dimension. Though both classical FF based MD and *ab* initio MD (AIMD) can be used for determining D, especially at dilute ionic concentrations, the use of AIMD is limited due to large computational cost associated with these simulations. We note that one should use a very accurate FF in MD simulations to compute D. The NEB approach is the most common approach and has been used extensively to study ion diffusion for various LIBs. Here, one considers several configurations, termed images, which connect the initial and final points along a predefined minimum energy path (MEP). These configurations are assumed to be connected by springs and the minimization of the images along with the springs provides the optimal MEP. Here, each of the image is a stationary point on the PES. However, this method is limited by the requirement of a predefined MEP (i. e. predefined initial and final states) and thus can be erroneous if multiple possible MEP are present. Moreover, finite temperature effects, which MD simulations accounts for, are not always included in NEB studies.

Studies over the years have identified two main ion hopping mechanisms for Li diffusion in layered metal oxides: Oxygen dumbbell hopping (ODH) and tetrahedral site hopping (TSH).[28k,44] The ODH pathway occurs in cases when all the sites near the vacancy to which Li hopping occurs are occupied. This forces the Li to choose a path across an oxygen dumbbell. TSH hopping occurs when Li adopts a curved path through a tetrahedral site.[28k,44] This pathway requires at least one di-vacancy near the site to which Li hops. Therefore, TSH pathways are preferred over ODH pathways at low Li concentrations.[28k,44] The increased feasibility of TSH pathway with increase in vacancy can be attributed to reduced repulsion between Li in the tetrahedral site and the TM in the nearby octahedral site.

2.4.2 Ion Diffusion in NCM

Hoang and Johannes studied diffusion in NCM333 using NEB with the HSE06 hybrid functional and found that ion diffusion in this material follows a mono-vacancy path in the fully lithiated limit, but follows a divacancy path at lower levels of

lithiation.[34] Experiments and PBE-based computations on NCM333 by Zhao et al. showed that cation exchange can block diffusion.[45] The decreased diffusion is ascribed to reduced Li-slab spacing due to cation exchange. The decreased diffusion or increased diffusion barrier with decrease in inter-slab spacing was also reported by Kang and Ceder in other Li transition metal oxides, such as LCO.[46] PBE computations by Dixit et al. on NCM523 focused on Li-migration via ODH and TSH pathways. In this study, the computed diffusion coefficient (3.6×10^{-11} cm^2s^{-1}) for the ODH pathway was found to be in agreement with the experimental diffusion coefficient (4.64×10^{-11} cm^2s^{-1}), whereas the diffusion coefficient computed for the TSH pathway was found to be much higher (8.6×10^{-5} cm^2s^{-1}).[28d] This indicates that the ODH pathway is the rate limiting one, whereas the TSH pathway is likely dominant at low Li-concentrations. The preference for the ODH pathway in the fully lithiated limit was also observed for NCM811 by Wei et al.[47] A diffusion coefficient of about 10^{-8} cm^2s^{-1} was determined in this study from AIMD simulation, in agreement with the experiments of Noh et al.[22b] These authors also compared the diffusion constant of Li in various NCM materials (Figure 5) and identified key factors influencing diffusion, such as Ni content, Ni valence states and Li-slab spacing.[47] Diffusion studies have also been employed to explain phase transitions. For example, Schipper et al. studied Ni interlayer migration using NEB calculations in conjunction with PBE to understand the layered to spinel phase transition in NCM622. Using DFT-based NEB calculations with the PBE functional the authors proposed a mechanism for layered to spinel phase transformation in this material.[26l] The authors suggested that layered-to-spinel transformation can be avoided by doping the material with a high-charge state cation, such as Zr^{4+}.[26l] This proposal was verified by experiments.

2.5 Doping in Layered Materials

Ni-rich NCM materials suffer from instability due to various phenomena such as cation mixing and phase transition, and consequently display capacity fading.[23] Doping of a foreign element in cathode materials is a very common and effective way to improve the performance of cathode materials. Dopants often improve the cycling stability by increasing the structural stability of NCM materials (e.g. by changing the Jahn-Teller active Ni^{3+} to Ni^{2+} ions), modify the lattice parameters and hence diffusion of Li-ions, and stabilize particle surfaces.[26l]

2.5.1 Methods

Study of doping in NCM is mostly done using DFT as is common in studies of pristine or undoped systems, as discussed above. It is important to note that accurately identifying dopant sites in host materials is very complicated through experiments, but it is apparently straightforward

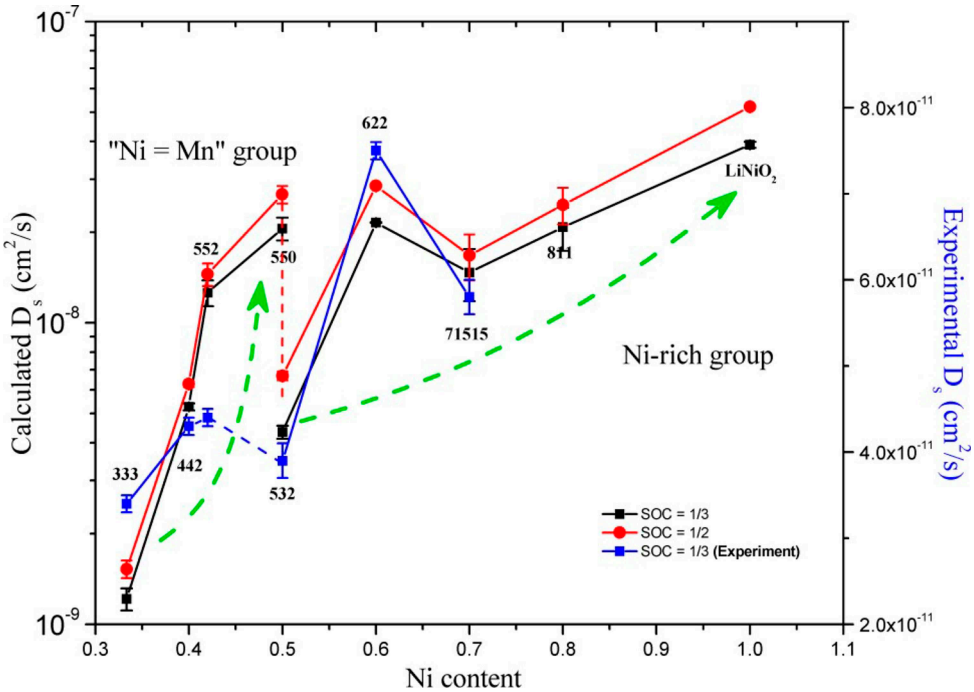

Figure 5. Diffusion coefficient (D_s), of different NMC materials for different states of charge computed from AIMD simulations and experiments. The statistical uncertainty in fitting of the MSD vs Time curve is shown as the error bar. (Reproduced from Ref. [47] with permission from the American Chemical Society)

theoretically from the calculation of formation energies. E.g. the formation energy for metal M' doped at Ni site is given by

$$FE = \left[E\left(\mathrm{LiM}'_p\mathrm{Ni}_{1-x-y-p}\mathrm{Co}_x\mathrm{Mn}_y\mathrm{O}_2\right) + p \cdot E(\mathrm{LiNiO}_2)\right] - \left[E\left(\mathrm{LiNi}_{1-x-y}\mathrm{Co}_x\mathrm{Mn}_y\mathrm{O}_2\right) + p \cdot E\left(\mathrm{LiM}'\mathrm{O}_2\right)\right]$$

Where $E(\mathrm{LiM}'_p\mathrm{Ni}_{1-x-y-p}\mathrm{Co}_x\mathrm{Mn}_y\mathrm{O}_2)$ and $E(\mathrm{LiNi}_{1-x-y}\mathrm{Co}_x\mathrm{Mn}_y\mathrm{O}_2)$ are the total energies of M′-doped NCM and undoped NCM materials. $E\left(\mathrm{LiM}'\mathrm{O}_2\right)$ and $E(\mathrm{LiNiO}_2)$ are the energies of the oxides of M' and Ni.

2.5.2 Doping in NCM

Many studies have addressed doping in NCM as we mentioned in section 1. Dixit et al. studied the effect of Al-doping in NCM523 using crystal orbital Hamilton population (COHP) analysis.[48] The authors noted that strong Al–O iono-covalency results in improved performance of the Al-doped material over the pristine material.[26f] They also noted an increase in the energy barrier height for Li-diffusion due to Al-doping in NCM523. Schipper et al. discussed the effect of Zr-doping in NCM622 and proposed that Zr preferably substitutes at Ni-sites using DFT calculations.[26f] They suggested that the high-valence nature of the dopant, Zr, yields a reduction in the number of Jahn-Teller active Ni^{3+} ions in NCM622, as observed from DFT calculations. This increase in Ni^{2+} at the expense of Ni^{3+} ions occurs to maintain charge neutrality in the system, and it may partly explain stabilization of the doped system.[26f] In this work, the barrier for cation mixing was found to be higher in the doped system than in the undoped one, based on NEB calculations. This could explain the experimentally observed inhibition of layered to spinel transformation.

Susai et al.[38] and Bruer et al.[26b] showed reduced capacity fading for NCM523 and NCM811 upon high-valence Mo-doping. Also, in these systems it was found that the high valence dopant, Mo, prefers Ni-sites, and hence results in an increase in the concentration of Ni^{2+} ions, as discussed above. They further observed reduction of charge transfer resistance from impedance spectroscopy for the Mo-doped NCM523 and NCM811. This can be attributed to the presence of additional electronic Mo-*d* bands in the conduction band region, as observed from the calculated DOS (Figure 6). The *c*-lattice parameter also increased upon doping of Mo in these NCMs, which may hinder cation mixing and hence increase the stability.[26b]

In another study, which examined the reasons for structural degradation in Ni-Rich NCMs, Dixit et al. performed comparative computational analysis of several layered NCMs and suggested that the oxidation state of Ni-ions determines the electrochemical activity and thermal stability of NCMs.[21b] The authors suggested that Ni^{2+} (i.e. Ni in 2+ oxidation state) is desirable due to ionic Ni – O interactions and availability of redox-active electrons.[21b,26l,28d] Additionally, it was suggested that Ni^{4+} ion imparts Ni–O covalency (due to a low-lying lowest unoccupied molecular orbital) which results in a propensity for reduction to Ni^{2+}, with concomitant oxygen release.[21b] The authors presented a high-valence cation doping strategy to reduce the oxidation state of Ni-ions in Ni-rich materials through charge compensation.

2.6 Surface Properties

In batteries, the surface of the electrodes reacts with electrolyte species and forms a solid electrolyte interphase (SEI). The SEI plays a crucial role in controlling rate capability, cyclic

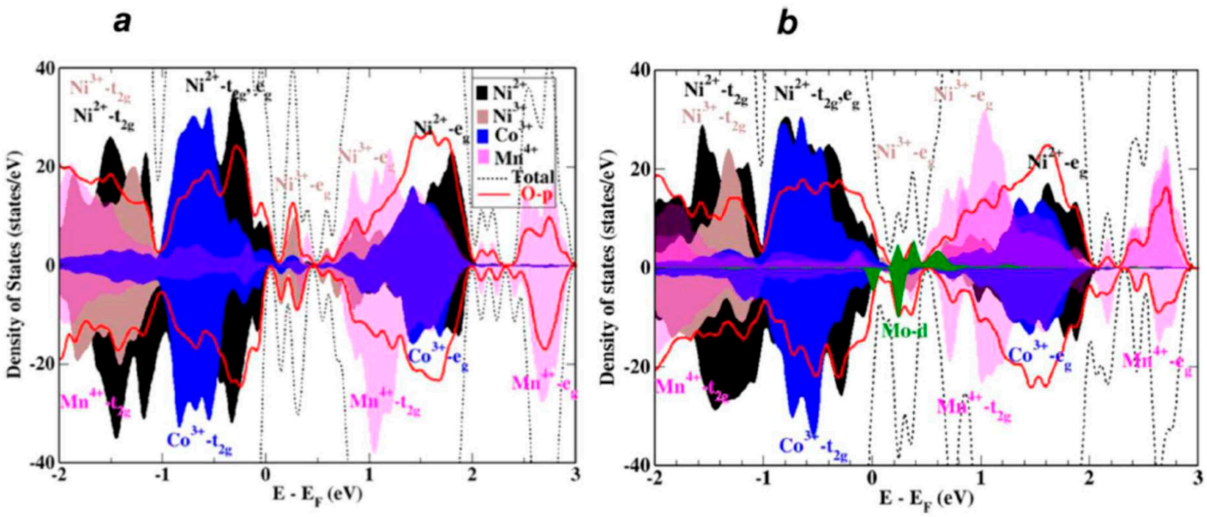

Figure 6. DOS for undoped (a) and Mo-doped (b) NCM523 samples. (Reproduced from Ref. [26b] with permission from the American Chemical Society).

performance etc. Hence, many computational studies have focused on surfaces of cathode materials.

2.6.1 Methods

Surface studies of NCMs have mostly employed the PBE+U method. The stable surface plane can be found from calculation of the surface energy (γ) using the following formula:

$$\gamma = \frac{E_{slab} - N \cdot E_{bulk}}{2A}$$

Here, E_{slab} and E_{bulk} are the total energies of the surface slab and bulk per formula unit. N and A are the number of formula units and area of the surface slab. The factor of 1/2 accounts for the two bare surfaces in the slab model (i.e. top and bottom of system).

2.6.2 Surface Studies for NCM

Electrolyte species react with surfaces of electrodes and form SEI. A commonly used electrolyte in LIBs is ethylene carbonate (EC). The reaction mechanism of EC at the layered oxide cathode surface is predominantly through ring opening followed by formation of oxygen vacancies at the surface. One can calculate reaction energies and barrier height for this surface reaction using the NEB method as performed by Østergaard et al.[49]

Recently it was also shown that surface coating in Ni-rich NCM can enhance the stability, and hence improve the electrochemical performance. Schipper et al. showed better cycling stability and lower impedance for ZrO_2 coating plus Zr-doping in NCM811 (Figure 7).[26k] They used the PBE functional for the NCM811(110):ZrO_2(001) interface to show that this interface has minimum strain. Importantly, this interface does not block any Li-diffusion channels and also improves the cycling stability.

Further, there are studies that show existence of additional structural phases, such as rock-salt, which coexist with the layered structure at the surface of layered materials.[23,50] It has been proposed that such rock-salt phases form in concert with release of oxygen.[23] Kong et al. showed from a combined theoretical and experimental work that release of oxygen is more predominant from the surface than the bulk region due to the higher kinetic barrier for oxygen migration in the bulk.[51] Kim et al. combined experiment and theory to show that W-doping of LNO resulted in formation of a rock-salt phase at the surface, which greatly improved capacity retention.[5f] They calculated surface energies for undoped and W-doped $LiNiO_2$ in both layered and rock-salt phases using the PBE+U method.

3. Summary and Outlook

In this review, we presented a brief overview of computational studies performed on Ni, Co and Mn based mixed transition metal layered oxide cathode materials (NCM) with the general formula $LiNi_{1-x-y}Co_xMn_yO_2$. Computational studies have provided atomic-level details of layered cathode materials that aid in rationalizing and designing experiments. The most common theoretical framework for studying NCM materials is DFT. Using DFT and other methods one can routinely compute a variety of properties, including structure, thermal stability, redox activities of the elements, intercalation voltages, plausible ion diffusion pathways, interface reactions between electrodes and electrolyte species, and energetics of oxygen release.

Layered NCM cathode materials have *R-3m* structure in the fully lithiated limit but may transform to inactive spinel or rock-salt structures upon cycling. Though Ni-rich NCMs provide high initial discharge capacity, these NCMs suffer from various problems, like cation disorder, oxygen release

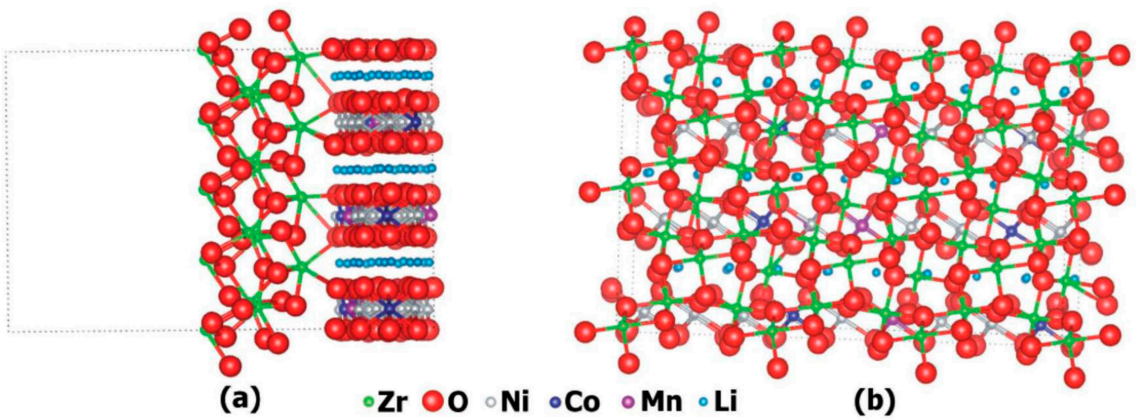

Figure 7. The interface models of a) side view and b) top view of the NCM811(110):ZrO2(001) interface. (Reproduced from Ref. [26k] with permission from Wiley)

and hence low stability on cycling, eventually causing capacity fading. Doping and surface coating can provide better stability and prolonged cycling for these materials. Theory is being used extensively to identify such dopants and coatings which can improve capacity retention in Ni-rich NCM materials. We believe that only through tight collaboration between experimentalists and theoreticians can one achieve the required mechanistic understanding that will eventually yield practical Ni-rich layered materials.

Acknowledgement

This work was partially supported by the Israel Science Foundation (ISF) in the framework of the INREP project.

References

[1] a) I. Dincer, *Renewable Sustainable Energy Rev.* **2000**, *4*, 157–175; b) O. Ellabban, H. Abu-Rub, F. Blaabjerg, *Renewable Sustainable Energy Rev.* **2014**, *39*, 748–764; c) J. Liu, J. G. Zhang, Z. Yang, P. Lemmon John, C. Imhoff, L. Graff Gordon, L. Li, J. Hu, C. Wang, J. Xiao, G. Xia, V. Viswanathan Vilayanur, S. Baskaran, V. Sprenkle, X. Li, Y. Shao, B. Schwenzer, *Adv. Funct. Mater.* **2012**, *23*, 929–946; d) P. A. Owusu, S. Asumadu-Sarkodie, *Cogent Eng.* **2016**, *3*, 1167990; e) N. L. Panwar, S. C. Kaushik, S. Kothari, *Renewable Sustainable Energy Rev.* **2011**, *15*, 1513–1524; f) M. M. Thackeray, C. Wolverton, E. D. Isaacs, *Energy Environ. Sci.* **2012**, *5*, 7854–7863.

[2] a) K. C. Divya, J. Østergaard, *Electr. Power Syst. Res.* **2009**, *79*, 511–520; b) B. Dunn, H. Kamath, J.-M. Tarascon, *Science* **2011**, *334*, 928; c) Z. Yang, J. Zhang, M. C. W. Kintner-Meyer, X. Lu, D. Choi, J. P. Lemmon, J. Liu, *Chem. Rev.* **2011**, *111*, 3577–3613.

[3] a) D. Deng, *Energy Sci. Eng.* **2015**, *3*, 385–418; b) J. B. Goodenough, Y. Kim, *Chem. Mater.* **2010**, *22*, 587–603; c) J. B. Goodenough, K.-S. Park, *J. Am. Chem. Soc.* **2013**, *135*, 1167–1176; d) Y. Nishi, *Electrochem. Soc. Interface* **2016**, *25*, 71–74; e) N. Nitta, F. Wu, J. T. Lee, G. Yushin, *Mater. Today* **2015**, *18*, 252–264; f) F. Schipper, E. M. Erickson, C. Erk, J.-Y. Shin, F. F. Chesneau, D. Aurbach, *J. Electrochem. Soc.* **2017**, *164*, A6220-A6228; g) B. Scrosati, J. Garche, *J. Power Sources* **2010**, *195*, 2419–2430; h) J. M. Tarascon, *Philos. Trans. R. Soc. London Ser. A* **2010**, *368*, 3227; i) J. M. Tarascon, M. Armand, *Nature* **2001**, *414*, 359; j) M. S. Whittingham, *Chem. Rev.* **2004**, *104*, 4271–4302; k) M. S. Whittingham, *Chem. Rev.* **2014**, *114*, 11414–11443.

[4] a) C. Liu, Z. G. Neale, G. Cao, *Mater. Today* **2016**, *19*, 109–123; b) N. Yabuuchi, K. Kubota, M. Dahbi, S. Komaba, *Chem. Rev.* **2014**, *114*, 11636–11682.

[5] a) B. L. Ellis, K. T. Lee, L. F. Nazar, *Chem. Mater.* **2010**, *22*, 691–714; b) E. M. Erickson, E. Markevich, G. Salitra, D. Sharon, D. Hirshberg, E. de la Llave, I. Shterenberg, A. Rosenman, A. Frimer, D. Aurbach, *J. Electrochem. Soc.* **2015**, *162*, A2424-A2438; c) V. Etacheri, R. Marom, R. Elazari, G. Salitra, D. Aurbach, *Energy Environ. Sci.* **2011**, *4*, 3243–3262; d) J. W. Fergus, *J. Power Sources* **2010**, *195*, 939–954; e) C. M. Hayner, X. Zhao, H. H. Kung, *Annu. Rev. Chem. Biomol. Eng.* **2012**, *3*, 445–471; f) U. H. Kim, D. W. Jun, K. J. Park, Q. Zhang, P. Kaghazchi, D. Aurbach, D. T. Major, G. Goobes, M. Dixit, N. Leifer, C. M. Wang, P. Yan, D. Ahn, K. H. Kim, C. S. Yoon, Y. K. Sun, *Energy Environ. Sci.* **2018**, *11*, 1271–1279; g) A. Kraytsberg, Y. Ein-Eli, *Adv. Energy Mater.* **2012**, *2*, 922–939; h) A. Manthiram, *J. Phys. Chem. Lett.* **2011**, *2*, 176–184; i) R. Marom, S. F. Amalraj, N. Leifer, D. Jacob, D. Aurbach, *J. Mater. Chem.* **2011**, *21*, 9938–9954; j) P. Rozier, J. M. Tarascon, *J. Electrochem. Soc.* **2015**, *162*, A2490–A2499; k) F. Schipper, K. P. Nayak, M. E. Erickson, F. S. Amalraj, O. Srur-Lavi, R. T. Penki, M. Talianker, J. Grinblat, H. Sclar, O. Breuer, M. C. Julien, N. Munichandraiah, D. Kovacheva, M. Dixit, T. D. Major, B. Markovsky, D. Aurbach, *Inorganics* **2017**, *5*, 32; l) X. Xu, S. Lee, S. Jeong, Y. Kim, J. Cho, *Mater. Today* **2013**, *16*, 487–495; m) W. Xu, J. Wang, F. Ding, X. Chen, E. Nasybulin, Y. Zhang, J.-G. Zhang, *Energy Environ. Sci.* **2014**, *7*, 513–537.

[6] a) C. Fang, X. Wang, Y. S. Meng, *Trends Chem.* **2019**, *1*, 152–158; b) C. Fang, J. Li, M. Zhang, Y. Zhang, F. Yang, J. Z. Lee, M.-H. Lee, J. Alvarado, M. A. Schroeder, Y. Yang, B. Lu, N. Williams, M. Ceja, L. Yang, M. Cai, J. Gu, K. Xu, X. Wang, Y. S. Meng, *Nature* **2019**, *572*, 511–515.

[7] S. L. Roselin, R.-S. Juang, C.-T. Hsieh, S. Sagadevan, A. Umar, R. Selvin, H. H. Hegazy, *Materials* **2019**, *12*.

[8] a) A. Abdellahi, A. Urban, S. Dacek, G. Ceder, *Chem. Mater.* **2016**, *28*, 5373–5383; b) S.-T. Myung, F. Maglia, K.-J. Park, C. S. Yoon, P. Lamp, S.-J. Kim, Y.-K. Sun, *ACS Energy Lett.* **2017**, *2*, 196–223; c) J. Zheng, S. Myeong, W. Cho, P. Yan, J. Xiao, C. Wang, J. Cho, J.-G. Zhang, *Adv. Energy Mater.* **2016**, *7*, 1601284; d) D. Zuo, G. Tian, X. Li, D. Chen, K. Shu, *J. Alloys Compd.* **2017**, *706*, 24–40.

[9] a) C. Delmas, C. Fouassier, P. Hagenmuller, *Physica B+C* **1980**, *99*, 81–85; b) M. S. Islam, C. A. Fisher, *Chem. Soc. Rev.* **2014**, *43*, 185–204; c) Y. S. Meng, M. E. Arroyo-de Dompablo, *Acc. Chem. Res.* **2013**, *46*, 1171–1180.

[10] M. D. Radin, S. Hy, M. Sina, C. Fang, H. Liu, J. Vinckeviciute, M. Zhang, M. S. Whittingham, Y. S. Meng, A. Van der Ven, *Adv. Energy Mater.* **2017**, *7*, 1602888.

[11] K. Mizushima, P. C. Jones, P. J. Wiseman, J. B. Goodenough, *Mater. Res. Bull.* **1980**, *15*, 783–789.

[12] W. Liu, P. Oh, X. Liu, M.-J. Lee, W. Cho, S. Chae, Y. Kim, J. Cho, *Angew. Chem. Int. Ed.* **2015**, *54*, 4440–4457; *Angew. Chem.* **2015**, *127*, 4518–4536.

[13] a) W. Li, J. N. Reimers, J. R. Dahn, *Phys. Rev. B* **1992**, *46*, 3236–3246; b) A. Manthiram, *ACS Cent. Sci.* **2017**, *3*, 1063–1069.

[14] M. Bianchini, M. Roca-Ayats, P. Hartmann, T. Brezesinski, J. Janek, *Angew. Chem. Int. Ed.* **2019**, *58*, 10434–10458.

[15] a) J. R. Dahn, U. von Sacken, M. W. Juzkow, H. Al-Janaby, *J. Electrochem. Soc.* **1991**, *138*, 2207–2211; b) M. G. S. R. Thomas, W. I. F. David, J. B. Goodenough, P. Groves, *Mater. Res. Bull.* **1985**, *20*, 1137–1146.

[16] a) H. Yu, Y. Qian, M. Otani, D. Tang, S. Guo, Y. Zhu, H. Zhou, *Energy Environ. Sci.* **2014**, *7*, 1068–1078; b) M.-H. Choi, C. S. Yoon, S.-T. Myung, B.-B. Lim, S. Komaba, Y.-K. Sun, *J. Electrochem. Soc.* **2015**, *162*, A2313-A2318.

[17] B. Ammundsen, J. Paulsen, *Adv. Mater.* **2001**, *13*, 943–956.

[18] a) Y. K. Sun, Y. S. Jeon, H. J. Leeb, *Electrochem. Solid-State Lett.* **2000**, *3*, 7–9; b) M. M. Thackeray, *Prog. Solid State Chem.* **1997**, *25*, 1–71.

[19] S. Komaba, N. Kumagai, Y. Kataoka, *Electrochim. Acta* **2002**, *47*, 1229–1239.

[20] a) T. Ohzuku, Y. Makimura, *Chem. Lett.* **2001**, *30*, 642–643; b) I. Saadoune, C. Delmas, *J. Mater. Chem.* **1996**, *6*, 193–199; c) E. Zhecheva, R. Stoyanova, *Solid State Ionics* **1993**, *66*, 143–149.

[21] a) A. R. Armstrong, P. G. Bruce, *Nature* **1996**, *381*, 499; b) M. Dixit, B. Markovsky, F. Schipper, D. Aurbach, D. T. Major, *J.*

Phys. Chem. C **2017**, *121*, 22628–22636; c) J. Xu, F. Lin, M. M. Doeff, W. Tong, *J. Mater. Chem. A* **2017**, *5*, 874–901.

[22] a) P. He, H. Yu, D. Li, H. Zhou, *J. Mater. Chem.* **2012**, *22*, 3680–3695; b) H.-J. Noh, S. Youn, C. S. Yoon, Y.-K. Sun, *J. Power Sources* **2013**, *233*, 121–130.

[23] S.-M. Bak, E. Hu, Y. Zhou, X. Yu, S. D. Senanayake, S.-J. Cho, K.-B. Kim, K. Y. Chung, X.-Q. Yang, K.-W. Nam, *ACS Appl. Mater. Interfaces* **2014**, *6*, 22594–22601.

[24] C. Liang, R. C. Longo, F. Kong, C. Zhang, Y. Nie, Y. Zheng, J.-S. Kim, S. Jeon, S. Choi, K. Cho, *J. Power Sources* **2017**, *340*, 217–228.

[25] a) B. Han, B. Key, S. H. Lapidus, J. C. Garcia, H. Iddir, J. T. Vaughey, F. Dogan, *ACS Appl. Mater. Interfaces* **2017**, *9*, 41291–41302; b) J. Kim, K. Amine, *J. Power Sources* **2002**, *104*, 33–39; c) J. Cho, Y. J. Kim, B. Park, *Chem. Mater.* **2000**, *12*, 3788–3791; d) J. Li, M. Fan, X. He, R. Zhao, C. Jiange, C. Wan, *Ionics* **2006**, *12*, 215–218; e) J. Li, Q. Zhang, C. Liu, X. He, *Ionics* **2009**, *15*, 493–496; f) J. Lu, Q. Peng, W. Wang, C. Nan, L. Li, Y. Li, *J. Am. Chem. Soc.* **2013**, *135*, 1649–1652; g) M. Aykol, S. Kirklin, C. Wolverton, *Adv. Energy Mater.* **2014**, *4*, 1400690.

[26] a) D. Aurbach, O. Srur-Lavi, C. Ghanty, M. Dixit, O. Haik, M. Talianker, Y. Grinblat, N. Leifer, R. Lavi, D. T. Major, G. Goobes, E. Zinigrad, E. M. Erickson, M. Kosa, B. Markovsky, J. Lampert, A. Volkov, J.-Y. Shin, A. Garsuch, *J. Electrochem. Soc.* **2015**, *162*, A1014-A1027; b) O. Breuer, A. Chakraborty, J. Liu, T. Kravchuk, L. Burstein, J. Grinblat, Y. Kauffman, A. Gladkih, P. Nayak, M. Tsubery, A. I. Frenkel, M. Talianker, D. T. Major, B. Markovsky, D. Aurbach, *ACS Appl. Mater. Interfaces* **2018**, *10*, 29608–29621; c) H. Cao, B. Xia, N. Xu, C. Zhang, *J. Alloys Compd.* **2004**, *376*, 282–286; d) C. H. Chen, J. Liu, M. E. Stoll, G. Henriksen, D. R. Vissers, K. Amine, *J. Power Sources* **2004**, *128*, 278–285; e) Y. Ding, P. Zhang, Y. Jiang, D. Gao, *Solid State Ionics* **2007**, *178*, 967–971; f) M. Dixit, B. Markovsky, D. Aurbach, D. T. Major, *J. Electrochem. Soc.* **2017**, *164*, A6359–A6365; g) H. Du, Y. Zheng, Z. Dou, H. Zhan, *J. Nanomater.* **2015**, *2015*, 5; h) G. Hu, M. Zhang, L. Liang, Z. Peng, K. Du, Y. Cao, *Electrochim. Acta* **2016**, *190*, 264–275; i) H. Kaneda, Y. Koshika, T. Nakamura, H. Nagata, R. Ushio, K. Mor, *Int. J. Electrochem. Sci.* **2017**, *12*, 4640–4653; j) H. Kondo, Y. Takeuchi, T. Sasaki, S. Kawauchi, Y. Itou, O. Hiruta, C. Okuda, M. Yonemura, T. Kamiyama, Y. Ukyo, *J. Power Sources* **2007**, *174*, 1131–1136; k) F. Schipper, H. Bouzaglo, M. Dixit, E. M. Erickson, T. Weigel, M. Talianker, J. Grinblat, L. Burstein, M. Schmidt, J. Lampert, C. Erk, B. Markovsky, D. T. Major, D. Aurbach, *Adv. Energy Mater.* **2018**, *8*, 1701682; l) F. Schipper, M. Dixit, D. Kovacheva, M. Talianker, O. Haik, J. Grinblat, E. M. Erickson, C. Ghanty, D. T. Major, B. Markovsky, D. Aurbach, *J. Mater. Chem. A* **2016**, *4*, 16073–16084; m) D. Wang, X. Li, Z. Wang, H. Guo, Y. Xu, Y. Fan, J. Ru, *Electrochim. Acta* **2016**, *188*, 48–56; n) J. Wu, H. Liu, X. Ye, J. Xia, Y. Lu, C. Lin, X. Yu, *J. Alloys Compd.* **2015**, *644*, 223–227.

[27] a) M. S. Islam, *Philos. Trans. R. Soc. London Ser. A* **2010**, *368*, 3255; b) A. Jain, Y. Shin, K. A. Persson, *Nat. Rev. Mater.* **2016**, *1*, 15004; c) S. Siqi, G. Jian, L. Yue, Z. Yan, W. Qu, J. Wangwei, O. Chuying, X. Ruijuan, *Chin. Phys. B* **2016**, *25*, 018212; d) A. Urban, D.-H. Seo, G. Ceder, *npj Comput. Mater.* **2016**, *2*, 16002; e) Y. Ma, *Energy Environ. Mater.* **2018**, *1*, 148–173.

[28] a) M. K. Aydinol, A. F. Kohan, G. Ceder, *J. Power Sources* **1997**, *68*, 664–668; b) M. K. Aydinol, A. F. Kohan, G. Ceder, K. Cho, J. Joannopoulos, *Phys. Rev. B* **1997**, *56*, 1354–1365; c) M. K. Y. Chan, C. Wolverton, J. P. Greeley, *J. Am. Chem. Soc.* **2012**, *134*, 14362–14374; d) M. Dixit, M. Kosa, O. S. Lavi, B. Markovsky, D. Aurbach, D. T. Major, *Phys. Chem. Chem. Phys.* **2016**, *18*, 6799–6812; e) S. Kirklin, B. Meredig, C. Wolverton, *Adv. Energy Mater.* **2013**, *3*, 252–262; f) Y. Mo, S. P. Ong, G. Ceder, *Chem. Mater.* **2012**, *24*, 15–17; g) K. Persson, V. A. Sethuraman, L. J. Hardwick, Y. Hinuma, Y. S. Meng, A. van der Ven, V. Srinivasan, R. Kostecki, G. Ceder, *J. Phys. Chem. Lett.* **2010**, *1*, 1176–1180; h) W. D. Richards, L. J. Miara, Y. Wang, J. C. Kim, G. Ceder, *Chem. Mater.* **2016**, *28*, 266–273; i) A. Van der Ven, M. K. Aydinol, G. Ceder, G. Kresse, J. Hafner, *Phys. Rev. B* **1998**, *58*, 2975–2987; j) A. Van der Ven, J. Bhattacharya, A. A. Belak, *Acc. Chem. Res.* **2013**, *46*, 1216–1225; k) A. Van der Ven, G. Ceder, *J. Power Sources* **2001**, *97–98*, 529–531; l) L. Wang, T. Maxisch, G. Ceder, *Chem. Mater.* **2007**, *19*, 543–552.

[29] A. M. Nolan, Y. Zhu, X. He, Q. Bai, Y. Mo, *Joule* **2018**, *2*, 2016–2046.

[30] a) J. Wilcox, S. Patoux, M. Doeff, *J. Electrochem. Soc.* **2009**, *156*, A192-A198; b) B. J. Hwang, Y. W. Tsai, D. Carlier, G. Ceder, *Chem. Mater.* **2003**, *15*, 3676–3682; c) Y. Koyama, I. Tanaka, H. Adachi, Y. Makimura, T. Ohzuku, *J. Power Sources* **2003**, *119–121*, 644–648.

[31] a) K. J. Harris, J. M. Foster, M. Z. Tessaro, M. Jiang, X. Yang, Y. Wu, B. Protas, G. R. Goward, *Chem. Mater.* **2017**, *29*, 5550–5557; b) A. van de Walle, *CALPHAD Comput. Coupling Phase Diagrams Thermochem* **2009**, *33*, 266–278; c) A. van de Walle, M. Asta, G. Ceder, *CALPHAD Comput. Coupling Phase Diagrams Thermochem* **2002**, *26*, 539–553.

[32] S. Lifson, A. Warshel, *J. Chem. Phys.* **1968**, *49*, 5116–5129.

[33] a) L. S. Cahill, S. C. Yin, A. Samoson, I. Heinmaa, L. F. Nazar, G. R. Goward, *Chem. Mater.* **2005**, *17*, 6560–6566; b) D. Zeng, J. Cabana, J. Bréger, W.-S. Yoon, C. P. Grey, *Chem. Mater.* **2007**, *19*, 6277–6289.

[34] K. Hoang, M. Johannes, *Chem. Mater.* **2016**, *28*, 1325–1334.

[35] A. Chakraborty, M. Dixit, D. Aurbach, D. T. Major, *npj Comput. Mater.* **2018**, *4*, 60.

[36] a) A. I. Liechtenstein, V. I. Anisimov, J. Zaanen, *Phys. Rev. B* **1995**, *52*, R5467-R5470; b) J. P. Perdew, K. Burke, M. Ernzerhof, *Phys. Rev. Lett.* **1996**, *77*, 3865–3868; c) J. Sun, R. C. Remsing, Y. Zhang, Z. Sun, A. Ruzsinszky, H. Peng, Z. Yang, A. Paul, U. Waghmare, X. Wu, M. L. Klein, J. P. Perdew, *Nat. Chem.* **2016**, *8*, 831.

[37] V. Singh, M. Kosa, K. Majhi, D. T. Major, *J. Chem. Theory Comput.* **2015**, *11*, 64–72.

[38] F. A. Susai, D. Kovacheva, A. Chakraborty, T. Kravchuk, R. Ravikumar, M. Talianker, J. Grinblat, L. Burstein, Y. Kauffmann, D. T. Major, B. Markovsky, D. Aurbach, *ACS Appl. Energy Mater.* **2019**, *2*, 4521–4534.

[39] a) J. van Elp, J. L. Wieland, H. Eskes, P. Kuiper, G. A. Sawatzky, F. M. F. de Groot, T. S. Turner, *Phys. Rev. B* **1991**, *44*, 6090–6103; b) F. Kong, R. C. Longo, M.-S. Park, J. Yoon, D.-H. Yeon, J.-H. Park, W.-H. Wang, S. Kc, S.-G. Doo, K. Cho, *J. Mater. Chem. A* **2015**, *3*, 8489–8500; c) S. Laubach, S. Laubach, P. C. Schmidt, D. Ensling, S. Schmid, W. Jaegermann, A. Thißen, K. Nikolowski, H. Ehrenberg, *Phys. Chem. Chem. Phys.* **2009**, *11*, 3278–3289.

[40] H. Sun, K. Zhao, *J. Phys. Chem. C* **2017**, *121*, 6002–6010.

[41] a) I. M. Markus, F. Lin, K. C. Kam, M. Asta, M. M. Doeff, *J. Phys. Chem. Lett.* **2014**, *5*, 3649–3655; b) B. Hwang, Y. Tsai, D. Carlier, G. Ceder, *Chem. Mater.* **2003**, *15*, 3676–3682; c) M. Dixit, M. Kosa, O. S. Lavi, B. Markovsky, D. Aurbach, D. T. Major, *Phys. Chem. Chem. Phys.* **2016**, *18*, 6799–6812; d) F. Schipper, M. Dixit, D. Kovacheva, M. Talianker, O. Haik, J. Grinblat, E. M. Erickson, C. Ghanty, D. T. Major, B. Markovsky, D. Aurbach, *J. Mater. Chem. A* **2016**; e) D.-H. Seo, A. Urban, G. Ceder, *Phys. Rev. B* **2015**, *92*, 115118.

[42] V. L. Chevrier, S. P. Ong, R. Armiento, M. K. Y. Chan, G. Ceder, *Phys. Rev. B* **2010**, *82*, 075122.

[43] A. Eftekhari, *ACS Sustainable Chem. Eng.* **2017**, *5*, 2799–2816.
[44] A. Van der Ven, J. C. Thomas, Q. Xu, B. Swoboda, D. Morgan, *Phys. Rev. B* **2008**, *78*, 104306.
[45] E. Zhao, L. Fang, M. Chen, D. Chen, Q. Huang, Z. Hu, Q.-b. Yan, M. Wu, X. Xiao, *J. Mater. Chem. A* **2017**, *5*, 1679–1686.
[46] a) K. Kang, G. Ceder, *Phys. Rev. B* **2006**, *74*, 094105; b) K. Kang, Y. S. Meng, J. Bréger, C. P. Grey, G. Ceder, *Science* **2006**, *311*, 977–980.
[47] Y. Wei, J. Zheng, S. Cui, X. Song, Y. Su, W. Deng, Z. Wu, X. Wang, W. Wang, M. Rao, Y. Lin, C. Wang, K. Amine, F. Pan, *J. Am. Chem. Soc.* **2015**, *137*, 8364–8367.
[48] a) V. L. Deringer, A. L. Tchougréeff, R. Dronskowski, *J. Phys. Chem. A* **2011**, *115*, 5461–5466; b) R. Dronskowski, P. E. Bloechl, *J. Phys. Chem.* **1993**, *97*, 8617–8624; c) S. Maintz, V. L. Deringer, A. L. Tchougréeff, R. Dronskowski, *J. Comput. Chem.* **2013**, *34*, 2557–2567.
[49] T. M. Østergaard, L. Giordano, I.E. Castelli, F. Maglia, B. K. Antonopoulos, Y. Shao-Horn, J. Rossmeisl, *J. Phys. Chem. C* **2018**, *122*, 10442–10449.
[50] C. Liang, R. C. Longo, F. Kong, C. Zhang, Y. Nie, Y. Zheng, K. Cho, *ACS Appl. Mater. Interfaces* **2018**, *10*, 6673–6680.
[51] F. Kong, C. Liang, L. Wang, Y. Zheng, S. Perananthan, R. C. Longo, J. P. Ferraris, M. Kim, K. Cho, *Adv. Energy Mater.* **2019**, *9*, 1802586.

Manuscript received: September 20, 2019
Revised manuscript received: November 7, 2019
Version of record online: ■■, ■■

REVIEW

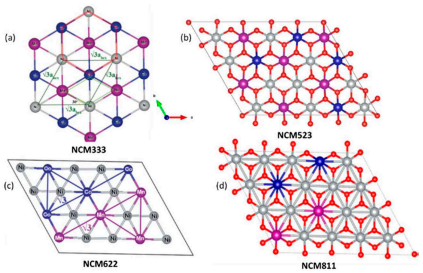

*A. Chakraborty, S. Kunnikuruvan, M. Dixit, D. T. Major**